Point defects in GaAs-$Ga_{1-x}Al_xAs$ superlattices

S. L. Feng, J. C. Bourgoin, and A. Mauger
Groupe de Physique des Solides de l'Ecole Normale Supérieure, Centre National de la Recherche Scientifique, Tour 23, 2 place Jussieu, 75251 Paris CEDEX 05, France

D. Stiévenard
Département de Physique des Solides, Institut Supérieur d'Électronique du Nord, 41 boulevard Vauban, 59046 Lille CEDEX, France

E. Barbier and J. P. Hirtz
Thomson–Laboratoire Central de Recherche, Boîte Postale 10, 91401 Orsay, France

A. Chomette
Centre National des Télécommunications, 22301 Lannion, France
(Received 8 December 1988)

Deep-level transient spectroscopy has been applied to the study of deep localized levels in a series of uniformly *n*-type-doped GaAs-$Ga_{1-x}Al_xAs$ superlattices having various periods. Using defects introduced by electron irradiation whose characteristics are well known in bulk GaAs and $Ga_{1-x}Al_xAs$, we demonstrate that their characteristics in these superlattices (energy-level position and majority-carrier capture cross section) can be reasonably predicted. We also show how the localization, which can be induced by the electric field, can be used to characterize native defects and eventually recognize them.

I. INTRODUCTION

Point defects play a leading role in semiconductor materials: they compensate and scatter the free carriers, shorten their lifetime, and introduce spurious effects. This is the case, for instance, of the famous EL2 defect in GaAs (for a recent review see Ref. 1) and *DX* center in $Ga_{1-x}Al_xAs$ (for a review see Ref. 2); the EL2 defect, commonly used to obtain semi-insulating materials, induces metastable effects at low temperature; as for the *DX* center whose presence is directly related to the *n*-type-doping impurity, it is at the origin of a persistent photoconductivity phenomenon. In heterostructures, which, in addition to point defects located in the layers contain interface defects between layers, the role of defects should be at least as important as in bulk materials. However, until now, practically no study has been performed in order to characterize these defects and to understand their behavior.

The aim of this study is to describe the electronic characteristics of point defects giving rise to deep levels in heterostructures. In particular, we shall examine how the defect characteristics, namely its associated electronic level(s) located in the forbidden gap, its carrier capture cross sections, and the optical cross sections from which all defect properties can be derived, can be deduced from the characteristics the same defect possesses in bulk material.

Actually, the case of simple heterostructures is not very interesting because the extension in space α^{-1} of the wave function of a deep defect is very small, namely of the order of 1 interatomic distance; defects located at a distance larger than α^{-1} from an interface are not perturbed. Consequently, their energy levels remain located at the same energy position in the layer as in the bulk material. This can be easily demonstrated using a first-order perturbation treatment (3). The shift ε in the energy level E_T of a defect located at a distance z from an interface characterized by a band offset Δ is

$$\varepsilon=\Delta\left[\frac{1+\alpha z}{2}\right]\exp(-2\alpha z)\ , \tag{1}$$

where the defect wave function decreases with increasing distance r as $\exp(-\alpha r)$. Typically ε/Δ is of the order of 10^{-2} for $\alpha z=2$. These results, namely that the energy level remains unperturbed when it is away from an interface, as well as the order of magnitude of the shift ε, have been verified using luminescence for the case of Mn in GaAs.[3,4]

Very recently Ren *et al.*[5] proposed a calculation of localized levels of impurities and defects in superlattices using a classical tight-binding approach with the aim of describing these level variations with the parameters which characterize the superlattice (the period and the alloy composition in the barrier) for $Ga_{1-x}Al_xAs$-GaAs structures. Unfortunately, they did not realize that (i) deep levels remain fixed within the original band structures of the materials which compose the superlattices, and their variations correspond directly to the changes in

the miniband structure, and (ii) each impurity or defect gives rise to two levels, one associated with the well, the other with the barrier. Moreover, because of the highly localized character of its wave function, a defect is not influenced by being embedded in a layer (except when it lies within α^{-1}, typically one interatomic distance, from an interface) and, consequently, is not sensitive to the new symmetry axis introduced by the superlattice periodicity. Their results should therefore be considered with caution since the nearest-neighbor tight-binding Hamiltonian they use cannot correctly describe the conduction band. This is well illustrated by the fact that they can obtain a deep level for the substitutional Si impurity which experimentally gives rise to a shallow level (otherwise Si-doped superlattices would not be n-type doped as demonstrated in this study).

The fact that a defect level remains unchanged, except for the defects located at one or two atomic distances from an interface, in the gap of the material which compose the layer, is very interesting when the band structure of the heterostructure is no more the band structure of the material which compose it. Indeed the defect can then play the role of a probe to study the new material. This new material is a superlattice in which the electrons can tunnel through the barriers resulting in a series of minibands in the direction perpendicular to the layers. We shall therefore concentrate our study on the case of superlattices.

We shall introduce defects, whose characteristics are known in the materials which compose the superlattice, in this superlattice in order to characterize it, namely to determine the band offset Δ and the band structure (the position of the bottom of the first miniband δ relative to the bottom of the well). We shall then investigate to what extent some of the characteristics (such as the carrier capture cross section) the defect has in the superlattice can be deduced from its characteristics in the original material which composes the well or the barrier. For this we have chosen the GaAs-$Ga_{1-x}Al_xAs$ system and we introduce the defects by electron irradiation. Indeed, electron irradiation allows us to introduce simple point defects in a controlled way, i.e., they are uniformly distributed and their concentration can be adjusted at will. Moreover, the characteristics of electron-induced defects in GaAs and, to some extent in $Ga_{1-x}Al_xAs$, have been extensively studied[6,7] and are reasonably well understood. In addition, because n-type-doped $Ga_{1-x}Al_xAs$ contains the DX center, superlattices containing doped $Ga_{1-x}Al_xAs$ barriers will allow us to study the effect of the band structure on the characteristics of this defect.

Only when this understanding is obtained does it become possible to characterize the native defects, i.e., the defects introduced during the growth or by technological processes. This will be done in Sec. VII.

II. THE HETEROSTRUCTURES

The structures studied are periodic GaAs-$Ga_{1-x}Al_xAs$ layers having the following well-barrier widths: 20-20 Å, 30-30 Å, 40-40 Å, 40-20 Å, and 50-50 Å, grown by molecular-beam epitaxy. In the text they will be labeled, respectively, (2,2), (3,3), (4,4), (4,2), and (5,5). The Al fraction in $Ga_{1-x}Al_xAs$ is $x=0.3$. Their thickness is 1 μm which means that they contain from 100 to 250 layers. The growth temperature is 600 °C; however, since the temperatures necessary to obtain the best quality GaAs and $Ga_{1-x}Al_xAs$ layers are different, this temperature has been sometimes modified to 650 °C in order to see its possible effect on the electrical properties of the structures. These structures are uniformly Si doped in order to provide a free-carrier concentration of the order of 10^{16} cm^{-3}. The growth is performed on n^+-type GaAs substrates in order to be able to make a good ohmic contact in the back of the structures. This contact is made by Ge- Ni deposition followed by a 450 °C anneal for 5 min. The top of the structure is a GaAs layer on which Schottky contacts are made by Al or Au deposition. In some cases Al Schottky barriers have been observed to contain interface states which have to be taken into account in the analysis of the C-V characteristics and of the deep-level transient spectroscopy (DLTS) spectra.

The C-V and C^{-2}-V characteristics at 300 K are given in Figs. 1 and 2 for all the structures studied. They provide uniform free-carrier concentrations n, typically equal to 2.5×10^{16} cm^{-3} [(2,2)], 3×10^{16} cm^{-3} [(3,3)], 1.5×10^{16} cm^{-3} [(4,4)], 3×10^{16} cm^{-3} [(4,2)], and 1×10^{16} cm^{-3} [(5,5)] for the structures which will mainly be used in this study. The measurements are performed with reverse biases in the range 0 to 5 V and thus allow us to obtain n in a depth ranging from 0.1–0.2 μm to 0.5–1 μm. These values of n are close to the values expected from Si introduction during growth.

The capacitance varies little with temperature (it decreases by about 20% from room temperature to 10 K), i.e., the carriers are not frozen up to 4 K because the capacitance measurements are performed at 1 MHz. This is also the case after electron irradiation, which is adjust-

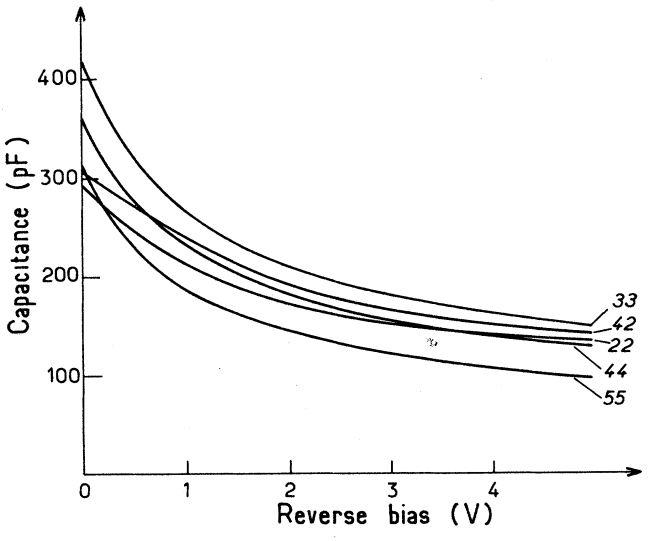

FIG. 1. Capacitance-voltage characteristics of the Schottky barriers made on the various structures.

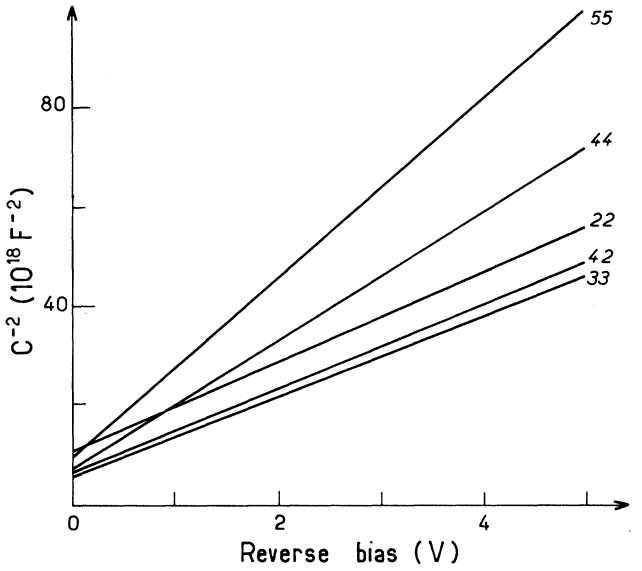

FIG. 2. Characteristics C^{-2}-V of the various structures showing that the doping concentration (provided by the slope of the characteristics) is uniform in the space-charge region.

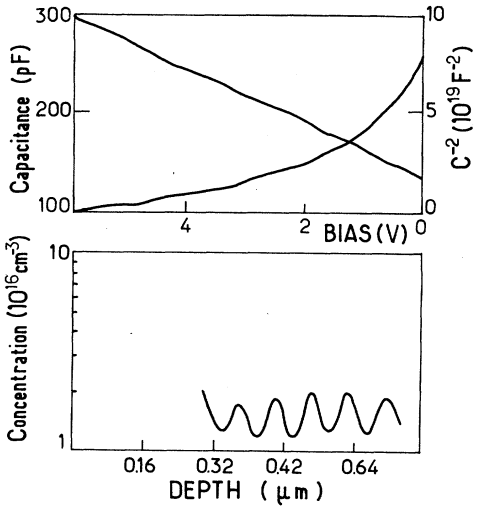

FIG. 3. C-V and C^{-2}-V characteristics of a 500-500 Å structure, from which the free-electron concentration vs depth is deduced.

ed to remove $\sim 10\%$ of the free carriers for all the structures except the (5,5) one in which the carriers appear to be frozen below ~ 30 K.

III. TECHNIQUE OF STUDY

The most effective spectroscopic technique to study deep levels in compound semiconductors is a technique based on the analysis of capacitance transients called deep-level transient spectroscopy. Indeed, luminescence applies mostly to the case of shallow donors and acceptors and radiative recombination is usually destroyed by the presence of deep levels which provide an effective nonradiative path for the recombination of electron-hole pairs. As to infrared absorption, it suffers the drawback of presenting large bands because deep defects in these materials are subject to strong electron-phonon interaction. As a result, DLTS, although limited in accuracy because it is a thermal spectroscopy, is the most effective and the most sensitive technique.

When a Schottky barrier or a junction is built on a doped superlattice with the electric field perpendicular to the layers, band bending occurs as in an homogeneously doped material since the band structure in this direction is made of minibands. Consequently, capacitance-voltage (C-V) measurements can be performed and analyzed as they are in the case of a bulk material, and it is possible to get the free-carrier density n as a function of the depth x from the slope of the C^{-2}-V curve.[8] This is illustrated in Figs. 1 and 2. This technique is also able to evaluate the localization of the carriers as illustrated in Fig. 3. In periodic 500-500 Å quantum wells, again uniformly doped with Si, the C-V characteristics exhibit oscillations which reflect the oscillations of the free-carrier concentration with the periodicity of the structure. Of course, because there is a transition region between a neutral zone and a depleted zone of the order of the Debye length

$$L_D=(\epsilon kT/q^2n)^{1/2} \tag{2}$$

(where ϵ is the dielectic constant of the material and q the electron charge), a change of n with x cannot be measured accurately when it occurs over a length smaller than L_D. In the case of Fig. 3 the Debye length is 400 Å at 300 K, i.e., of the same order of magnitude as the width of the wells. However, L_D can be substantially decreased by lowering the temperature ($L_D \simeq 50$ Å at 4 K).

The electric field F varies linearly in the space charge region from zero at $x=W$, the limit of the space charge region, to typically 10^4 V cm^{-1} at $x=0$, the barrier interface (reverse biases are of the order of 1 V for space charge region of the order of 1 μm, with the doping concentration used, $n \sim 10^{16}$ cm^{-3}). Therefore it can induce electronic localization when qFd (d is the period of the superlattice) is larger than the width of the miniband. This can be put in evidence using DLTS because the carriers localized in the wells can then be emitted above the barriers, giving rise to a series of peaks in the DLTS spectrum. Because the barrier for the emission is (see Fig. 4) $\Delta-\delta-qFd/2$ (δ is the energy position of the miniband measured from the bottom of the well), there is a sequence of peaks of energies separated by $q\,dF\,d$, dF being the change of F from one well to an adjacent one. This phenomenon has been observed clearly in structures (5,5) (Fig. 5) and can also be apparent in other structures [such as the (4,2) one] in which the widths of the first miniband are smaller than in the (2,2), (3,3), and (4,4) structures (see Table I). A detailed interpretation of these spectra is given in Ref. 9. We shall see in the last section that one

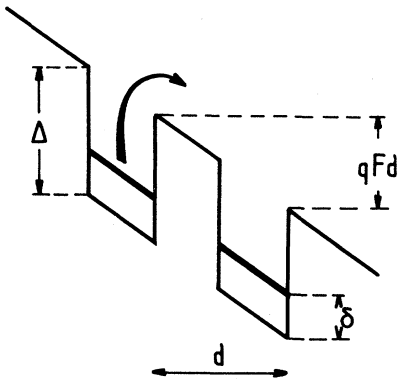

FIG. 4. Schematic representation of the emission of an electron localized on the level δ of a well of depth Δ placed in an electric field F.

can take advantage of this phenomenon to identify native defects since, in the region of the space charge region where the localization occurs, the miniband being destroyed, the original band structure of the materials which compose the layers is restored and the defects exhibit the same DLTS spectra as in the bulk material.

This localization effect does not perturb capacitance measurements. They are performed by a small modulation of the reverse bias (usually few meV at 1 MHz), i.e., of the edge of the space charge region. Since the electric field in this region is extremely small, the carriers remain delocalized.

In a superlattice carrier emission occurs from the localized state into the bottom of the first miniband. DLTS provides the variation of the emission rate versus temperature from which one gets the ionization energy E_i of the defect, i.e., its location compared to the bottom of the first miniband δ. Thus (see Fig. 6), when the level, located at E_T below the conduction band of the original material, is in the well

$$E_{iw}=E_T+\delta\ . \tag{3}$$

When it is located in the barrier

$$E_{ib}=E_T-\Delta+\delta\ . \tag{4}$$

The emission rate contains the carrier capture cross section σ_c in the preexponential term. Because, for deep levels, the capture occurs through multiphonon emission, it can happen that in the temperature range where the measurements are performed, σ_c varies as

$$\sigma_c=\sigma_\infty\exp(-B/kT) \tag{5}$$

and the ionization energy

$$E_i=E_T+B \tag{6}$$

must be corrected for the existence of the barrier B in order to get E_T. This can be done by independently measuring σ_c and its variation with temperature through a study of the filling kinetics.

Finally, one must take care of the fact that the emission can be enhanced by the electric field. This phenomenon is due to the fact that, when the electron-phonon interaction is strong enough, emission can also occur by phonon assisted tunneling. This phenomenon results in a distortion of the DLTS peak providing an apparent ionization energy and defect concentration lower than the real ones. Its existence can be checked by looking at the variation of the emission rate of the defects placed in different parts of the space charge region. In the case of the superlattice studied here, this effect has been looked for on all the defects observed in all the structures but found to be negligible.

For all the reasons described above the characteristics of a defect cannot be extracted directly from the DLTS spectrum and the few DLTS studies which have been described so far[10,11] should be considered with caution.

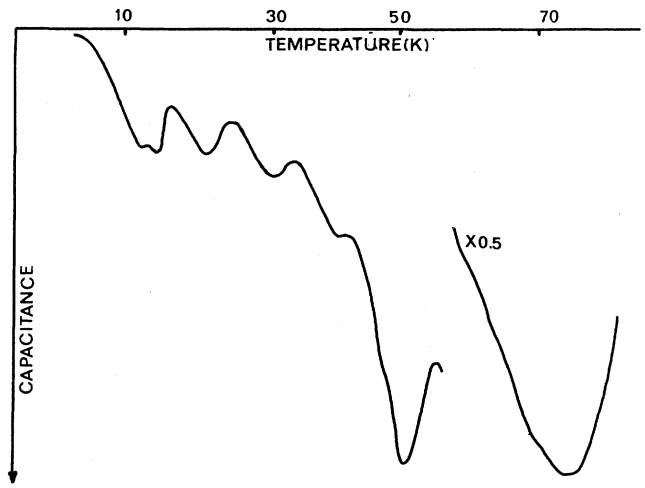

FIG. 5. Low-temperature (4–100 K) DLTS spectrum observed in a (5,5) structure.

IV. CHARACTERIZATION OF ELECTRON-INDUCED DEFECTS

Irradiation is performed at room temperature. The electron beam is scanned over an area which is large compared to the sample surface in order to insure a

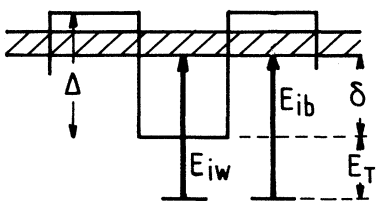

FIG. 6. Electron emission (E_{iw} and E_{ib}) from a level, located, respectively, at E_T and $E_T+\Delta$ below the conduction bands of the materials which compose the well and the barrier, into the bottom of the superlattice miniband (situated at δ above the bottom of the well band).

TABLE I. Calculated (see Sec. V) energy (bottom) positions δ_j (meV) and widths $\omega\delta_j$ (meV) of the j minibands (meV) in the various structures studied.

Structures (Å)	(2,2)	(3,3)	(4,4)	(4,2)	(5,5)
δ_1	127.9	113.1	95.9	74.2	79.3
$\omega\delta_1$	198.8	65.5	22.8	78	8
δ_2	492.9				248.3
$\omega\delta_2$					

homogeneous irradiation. The energy of irradiation, 1 meV, is such that the energy lost in the thickness of the structures ($\sim$5 keV) is negligible; thus, the defect introduction rate is uniform over the whole depth. Since the introduction rates of the various defects induced in GaAs and $Ga_{1-x}Al_xAs$ are known, it is easy to adjust the fluence received so that the total concentration of the defects which trap free electrons remains equal to 10% of the free-electron concentration. This way the change ΔC in the capacitance C introduced by electron emission from the defects remains such that $\Delta C/C < 2.5\times10^{-2}$ and the DLTS analysis remains simple, without the need for corrections.

Typical DLTS spectra obtained in each structure are shown in Figs. 7(a)–7(d). Electron irradiation induces a series of four peaks which are labeled *SE*1 to *SE*4 in increasing order of temperature. The (5,5) structure already contains a number of peaks prior to irradiation (see Fig. 5); however, the electron-induced peaks can be well separated since their amplitudes are, in most cases, considerably larger. The ionization energies of each of these irradiation-induced peaks has been measured from the slopes of the logarithm of the emission rate versus the inverse of the temperature (see Fig. 8). The results are given in Table II.

The capture kinetics of all these traps have been deter-

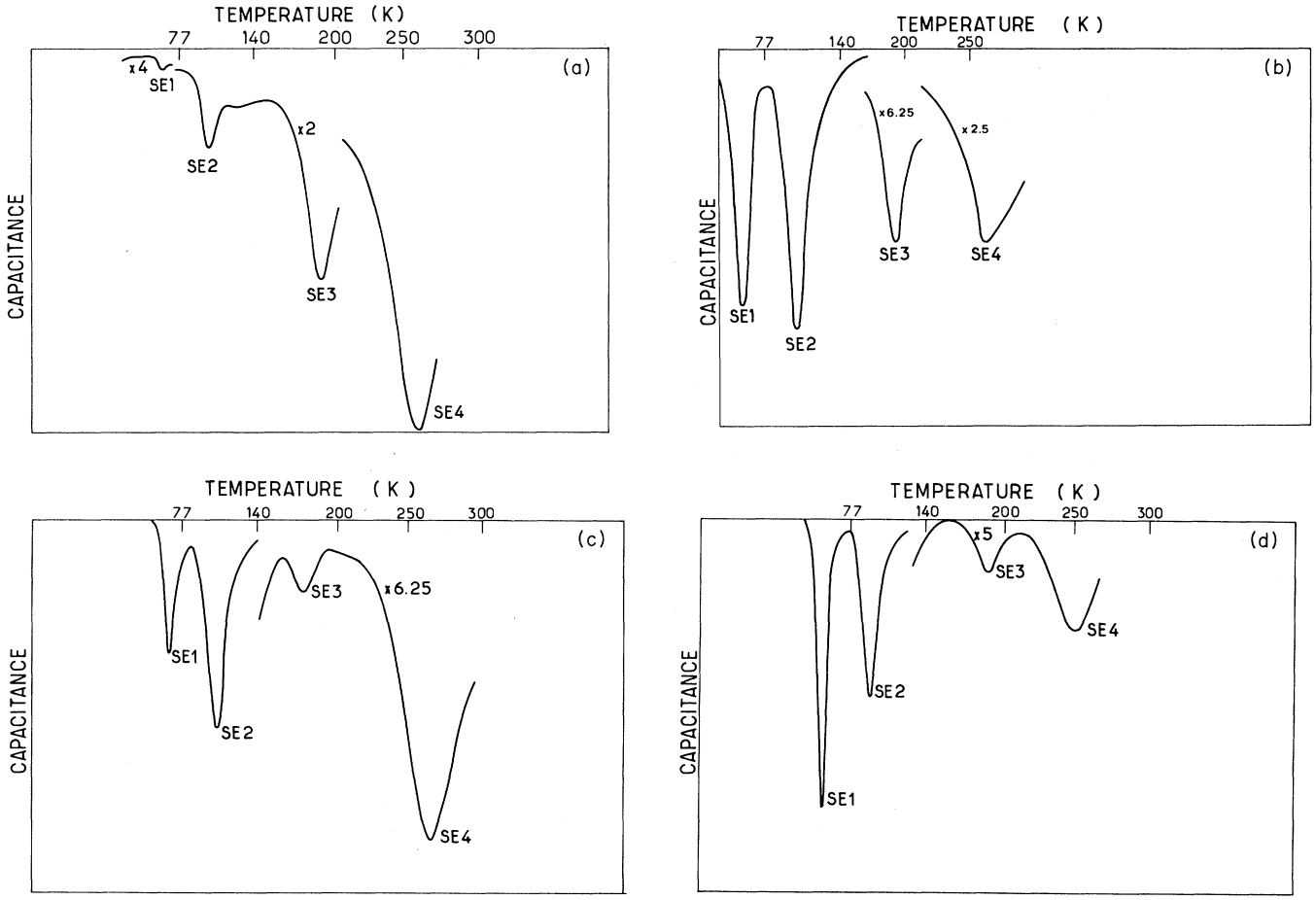

FIG. 7. DLTS spectra obtained in the electron irradiated structures: (a) (5,5) (emission rate 46.2 s^{-1}); (b) (4,4) (emission rate 53.25 s^{-1}); c (3,3) (emission rate 10.65 s^{-1}); (d), (4,2) (emission rate 42.6 s^{-1}). The DLTS spectrum of the (2,2) structure can be found in Ref. 12.

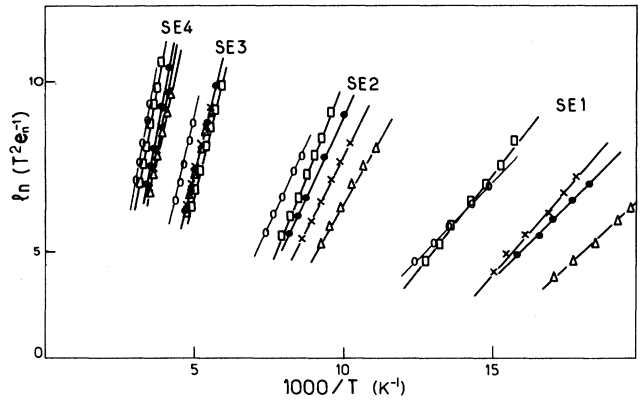

FIG. 8. Variation of the emission rate e_n vs the inverse of the temperature for the four peaks ($SE1$–$SE4$) introduced by the irradiation in the various structures: 0, (2,2); □, (3,3); △, (4,2); ○, (4,4); ×, (5,5).

mined by monitoring the amplitudes of the peaks (proportional to the concentration n_t of filled traps) as a function of the filling pulse duration t_p. Typical examples are shown in Fig. 9. The capture kinetics are given by

$$n_t = N_T[1-\exp(-C_n t_p)] \ . \tag{7}$$

The plot of $\ln[(N_T-n_t)/N_T]$ should be linear with t_p and the slope can provide the capture rate C_n from which one can deduce the capture cross section σ_n. The total concentration of traps N_T is given by the saturating value of $n_t(t_p)$ for long times. In most cases, the plot $\ln[(N_T-n_t)/N_T]$ versus t_p is not linear (see typical examples in Fig. 10) because, for long times, the capture rate reflects the filling in the Debye tail at the edge of the space charge region. For this reason we have calculated σ_n using the data corresponding to low values of t_p. The variations of σ_n with the inverse of temperature, given in Figs. 11(a)–11(c), are then determined by changing the value of the emission rate at which the variations $A(t_p)$ are recorded. Owing to the small temperature range in which the peaks can be observed, the activation energy B associated with this capture cross section [see expression (4)], measured from the slope of $\ln(\sigma_n)$ versus T^{-1} (Fig. 11) often cannot be determined with good accuracy. The results are given in Table III. When a capture cross section is too small to be measured, i.e., when it gives rise to

TABLE II. Ionization energies (meV) for the electron-induced traps observed in the various structures.

Structure	$SE1$	$SE2$	$SE3$	$SE4$
(2,2)	91±4	243±5	354±19	519±48
(3,3)	118±5	223±5	372±4	505±27
(4,4)	88±4	208±15	366±18	461±50
(4,2)	77±4	154±6	321±28	465±4
(5,5)	101±4	179±4	368±12	465±14

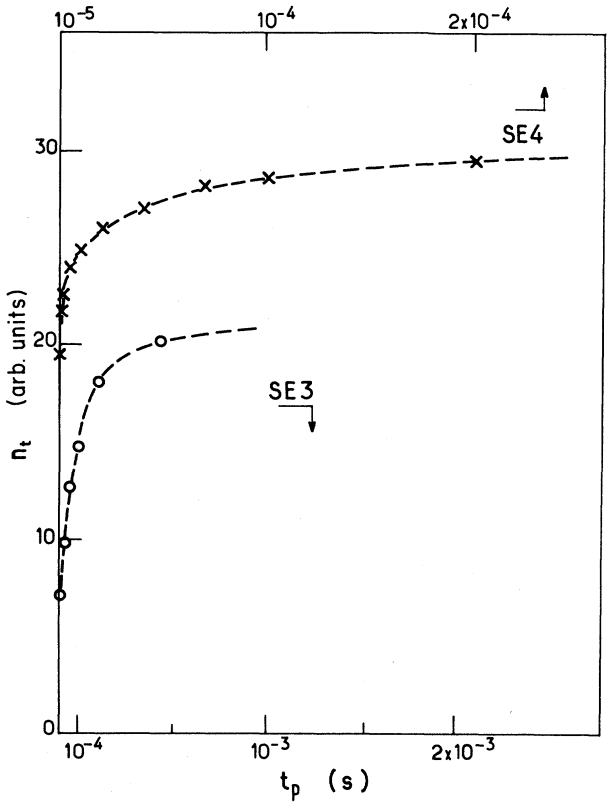

FIG. 9. Variations of the concentrations n_t of the filled $SE3$ and $SE4$ traps in arbitrary units vs the filling time t_p in a (4,4) structure (emission rate 53.3 s^{-1}).

a capture time constant smaller than, typically, 10 μs in the whole temperature range, we have taken $B=0$ since, if B is not zero, it remains nevertheless small, of the order lower than the accuracy of the measurements. Indeed, if B were larger it would give rise to a measurable capture time constant in the high-temperature range. Finally, Table IV summarizes the concentrations of the different traps, as measured from the amplitude of the corresponding peaks, obtained for an irradiation dose equal to $0.1n$.

V. DEFECT CHARACTERISTICS—DISCUSSION

A. Energy levels

We obtain the location of the energy level of the defect E_T^S below the minimum δ_1 of the first miniband from independent DLTS measurements of the ionization energy E_i^S and of the barrier height B_S associated with the capture cross section, through an expression similar to (6):

$$E_T^S = E_i^S - B_S \ . \tag{8}$$

As to the energy position within the original band structure, it depends if this defect lies in a barrier or in a well. It is deduced using expressions (3) or (4), once the quantities Δ and δ_1 are known.

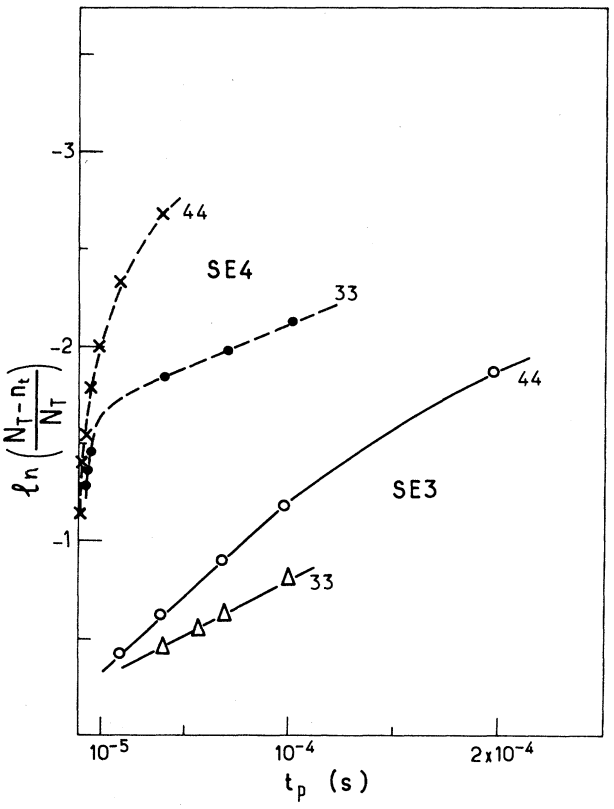

FIG. 10. Variation of the logarithm of the fraction of filled traps vs the filling time t_p for the $SE3$ and $SE4$ traps in the (3,3) and (4,4) structures.

Fortunately, because the energy positions of the electron-induced defects are known in GaAs (Ref. 6) and $Ga_{1-x}Al_xAs$,[7,12] as well as the corresponding barriers for electron capture (see Table V), it is possible to ascribe each of the E_T^S values for the defects to the well or the barrier and thus to deduce both the values of Δ and δ_1. Indeed, the energy difference between two defect levels ($E1$ to $E3$ in GaAs and $E'1$ to $E'3$ in $Ga_{1-x}Al_xAs$, for instance) are the same in the original materials and in the superlattice. According to expressions (3) and (4) we can, in principle, deduce the energy levels in the superlattice from the energy levels the same defects have in GaAs and $Ga_{1-x}Al_xAs$, from an energy shift δ_1 or $\Delta-\delta_1$, respectively. This has already been done in the case of the (2,2) structure.[13] Here we perform the same analysis but for all the structures and we compare the values we deduce for δ_1 and Δ with the calculated values of δ_1 versus Δ (Fig. 12) in order to get a consistent picture for all these structures. The calculation of the superlattice band structures is made using the Kroening-Penney model described in Refs. 4 and 14. The way we proceeded to obtain the fit is the following. First, δ_1 is calculated for different values of Δ and the expected energy levels of the different defects in the superlattices are calculated using expressions (3) and (4) using the values of the defect energy levels in GaAs and $Ga_{1-x}Al_xAs$. These calculated values are then compared with the experimental ones. The comparison provides the value of Δ which fits the set of data. This way the fit is automatically in agreement with the theoretical values for δ_1. In Table VI we show the calculated energy levels which best fit the experimental values given in Table VII for $\Delta=280$ meV. It can be shown that $SE1$ corresponds to $E1$, $SE2$ to $E2$, $SE3$ to $E'2$, and $SE4$ to $E3$; $E'1$ is not observed because it is resonant in the miniband or very close to the band edge (in which case the emission proceeds below the minimum temperature we used). The fit is good for the $SE2$ and $SE4$ levels which presumably involve $E'3$ in addition to $E3$. It is reasonably good for $SE3$ except in case of the (2,2) structure; obviously the reason is that the experimental value of B_S taken to deduce E_T^S from the ionization energy is too small in this case (it is between 255 and 300 meV for the other structures).

In conclusion, one can reasonably well fit the experimental results observed, which means that the picture we have assumed, namely that the energy levels of the defects remain linked to the original band structures of the materials which compose the superlattice, is verified. The fit is in agreement with the band structure calculation used. This provides a measurement of the band

TABLE III. Activation energy B_S (meV) associated with electron capture cross section for the electron-induced traps in the various structures.

Structure	$SE1$	$SE2$	$SE3$	$SE4$
(2,2)	0	0	44±14	26±6
(3,3)	0	0	269±80	61±13
(4,4)	0	0	265±80	58±12
(4,2)	0	0	265±80	62±13
(5,5)	0	0	298±90	52±10

TABLE IV. Introduction rates (cm^{-1}), i.e., defect concentrations divided by the irradiation dose of the defects in the various structures induced by 1 meV electron irradiation.

Structures	(2,2)	(3,3)	(4,4)	(4,2)	(5,5)
$SE1$	0.5	0.22	0.67	0.57	0.004
$SE2$	0.5	0.43	0.73	0.43	0.04
$SE3$	0.02	0.26	0.08	0.05	0.13
$SE4$	0.1	0.13	0.23	0.22	0.60

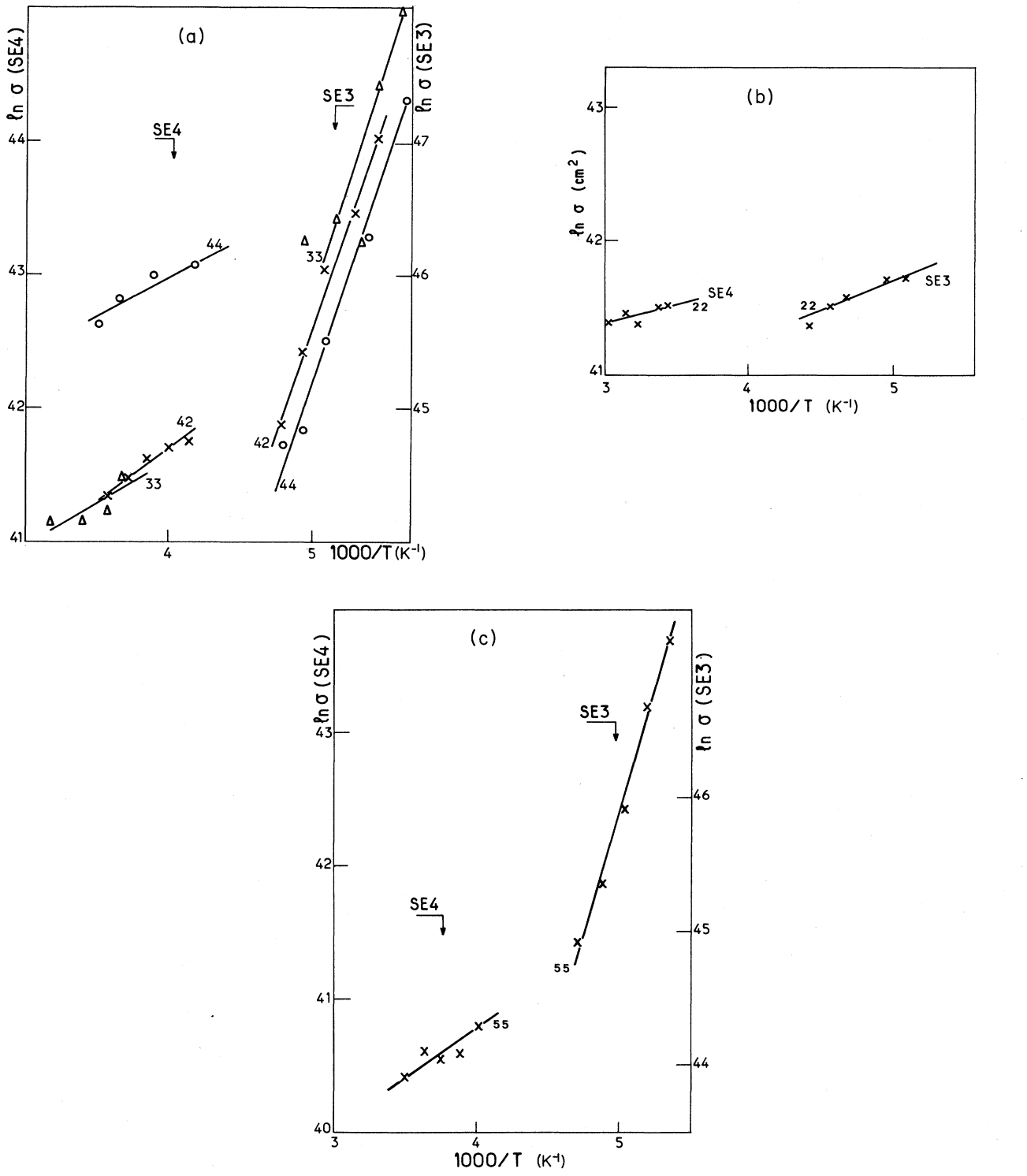

FIG. 11. Variations (logarithmic scale) of the capture cross sections (cm^2) of the *SE*3 and *SE*4 traps vs the inverse of the temperature in the (a) (3,3), (4,2), and (4,4), the (b) (2,2), and (c) (5,5) structures.

offset, here 70%, a value in agreement with other determinations which vary between 60% and 75% (a full discussion of the electrical methods for band-offset determination will be developed elsewhere).

B. Introduction rates

The introduction rates of the four traps observed in all the structures are given in Table IV. They have been

TABLE V. Energy levels E_T (meV), associated barriers B (meV), Franck-Condon shift d_{FC} (meV), and introduction rate R normalized to $E2$ or $E'2$ for the defects induced by electron irradiation in GaAs (E_i,B_i) and $Ga_{1-x}Al_xAs$ (E_i',B_i'), respectively. In the case of GaAs the E and B values have been determined from a study of GaAs layers performed exactly in the same conditions as for the superlattices, with a material having a similar free-carrier concentration (1×10^{16} cm^{-3}). For this reason the (apparent) E_T values given are different from the exact values given in Ref. 6. In the case of $Ga_{1-x}Al_xAs$ the values have been taken from Refs. 6 and 11, using, when necessary, a linear extrapolation vs alloy composition x between two values of x (0.25 and 0.35) adjacent to $x=0.3$.

	E_T	B	R	d_{FC}
		GaAs		
$E1$	22	0	1	0.38
$E2$	94	?	1	0.22
$E3$	313	80	0.25	0.20
		$Ga_{1-x}Al_xAs$		
$E'1$	180	?	0.75	?
$E'2$	270	?	1	?
$E'3$	690	140	0.35	?

measured using the same emission-rate window (42.6 s^{-1}) and a pulse width t_p equal to 10% of the period ($t_p=5$ ms). For these values all the traps are practically filled. The fact that the $SE1$ and $SE2$ defects exhibit the same concentration [except in the (5,5) structure, presumably because of the localization induced by the electric field], verifies the correspondence deduced above since the $E1$ and $E2$ levels are two charge states of the same defect.[5] The introduction rates of the $SE1$, $SE2$, and $SE4$ defects are, within 100% accuracy, those expected, i.e., 0.5 times [0.66 for the (4,2) structure] the $E1$, $E2$, and $E3+E'3$ concentrations, respectively, except for the (5,5) structure. However, the concentration of $SE3$, i.e., in $Ga_{1-x}Al_xAs$, is smaller than expected. Once again, it is not surprising that the order of magnitude of the introduction rates in the (5,5) structure are not those expected since, as discussed in Sec. III, a localization is induced by the electric field in a large part of the space charge region.

Thus, owing to the inaccuracy introduced by several effects, such as partial localization, uncomplete filling of the traps and perhaps others such as the enhancement of the emission by phonon assisted tunneling (which is small since not detected on the variation of the emission rate with temperature but which can be sufficiently high to decrease the apparent concentration) the introduction rate data can be considered as being in agreement with the assignments between the SE defects and the E and E' ones, deduced in Sec. V A.

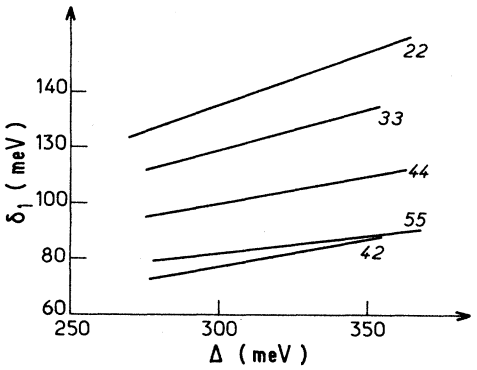

FIG. 12. Variation of the position of the bottom δ_1 of the first miniband above the energy of the well vs the well depth Δ.

C. Capture cross sections

Nonradiative capture on deep levels occurs via the multiphonon emission process characterized by the energetic barrier B in expression (4). In classical terms this energy can be viewed as the barrier an electron in the conduction band must overcome in order to get trapped on the defect site. This is commonly represented in the configuration coordinate diagram (see Fig. 13) representing the variation versus a configuration coordinate Q of the total energy (the sum of the electronic and vibrational energies) of the defect when it is filled $E_f(Q)$ and empty $E_e(Q)$, i.e., with the electron in the conduction band. These energies can be written

$$E_f^{(Q)}=\tfrac{1}{2}kQ^2 \tag{9}$$

and

$$E_e^{(Q)}=\tfrac{1}{2}kQ^2-(E_T-d_{FC})-IQ\ , \tag{10}$$

where k is a local force constant, d_{FC} the Franck-Condon shift, and I the electron-phonon interaction. The barrier

TABLE VI. Calculated values of the E_T^S energy levels (meV) in the structures studied for a band offset of 70% ($\Delta=280$ meV).

Structures	(2,2)	(3,3)	(4,4)	(4,2)	(5,5)
$E'1$	28	13	4		
$E'2$	118	103	86	69	64
$E'3$	538	522	506	489	484
$E1$	160	135	117	101	96
$E2$	222	207	190	173	168
$E3$	441	426	409	394	387

TABLE VII. Experimental defect energy levels E_T^S in the various structures as deduced from the difference between their ionization energy E_i^S and the barrier for capture B_S given in Tables II and III, respectively.

Structure	*SE*1	*SE*2	*SE*3	*SE*4
(2,2)	91	243	310	493
(3,3)	118	223	103	444
(4,4)	88	208	101	403
(4,2)	77	154	56	403
(5,5)	101	179	70	413

B is then the value of E_f at the abscissa where both curves cross. It is given by

$$B=\frac{k}{2I^2}(d_{FC}-E_T)^2 . \tag{11}$$

When the conduction band of the material in which the defect is embedded is replaced by a miniband, the energy of the free electron is shifted from a value K equal to δ for a defect in a well and to $-\Delta+\delta$ for a defect in a barrier. The defect total energy is in that case

$$E_{SL}(Q)=\tfrac{1}{2}kQ^2+K \tag{12}$$

because, the defect being localized, the local force constants are not perturbed by introducing the defect in a layer. Consequently, the capture barrier height in the superlattice becomes

$$B_S=\frac{k}{2I^2}(d_{FC}-E_T-K)^2 . \tag{13}$$

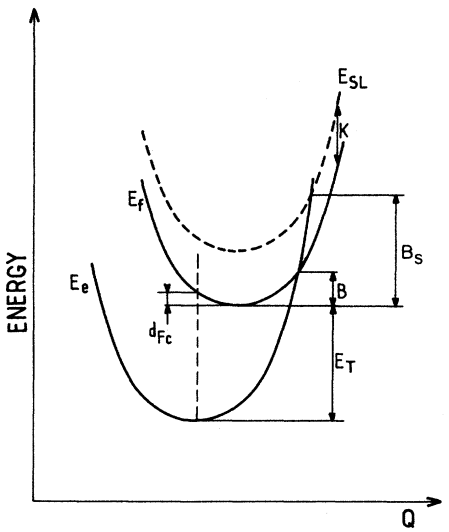

FIG. 13. Configuration coordinate diagram of a defect exhibiting a non-negligible electron-phonon interaction whose amplitude is given by the Franck-Condon shift d_{FC}. E_e, E_f, and E_{SL} represent the defect total energy with the electron, respectively, on the defect site, in the conduction band of the material which composes the well or the barrier, and in the superlattice miniband. The barriers for the recombination of an electron situated in the material band and in the superlattice miniband on the defect level (E_T) are B and B_S, respectively.

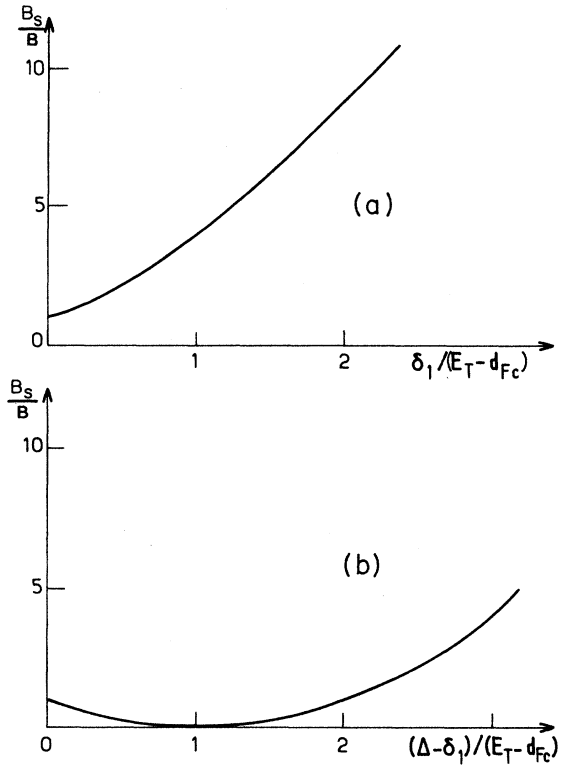

FIG. 14. Variation of the ratio B_S/B vs $K/(E_T-d_{FC})$ for a defect (a) in a well ($K=\delta_1$) and (b) in a barrier ($K=\Delta-\delta_1$).

Eliminating k/I^2 between expressions (10) and (12), one obtains the following simple relation between B_S and B:

$$\frac{B_S}{B}=\left[1+\frac{K}{E_T-d_{FC}}\right]^2 , \tag{14}$$

whose variation versus the ratio $K/(E_T-d_{FC})$ is depicted in Fig. 14.

Since some of the barriers B for the various electron-induced defects are reasonably known, it is possible to verify if the above considerations apply and consequently if the correspondence between the E, E' and the E_T^S defects we have determined is correct.

Consider first the *SE*1 and *SE*2 defects, which we determined to originate from the $E1$ and $E2$ defects in GaAs. For these defects $B=0$ and we indeed find experimentally $B_S=0$. In the case of *SE*3, originating from the $E'2$ defect in $Ga_{1-x}Al_xAs$, B is unknown. Finally, in the case of *SE*4, B_S values are lower than the B value of the $E3$ defect which implies that expression (13) cannot be applied using $K=\delta_1$. However, if the *SE*4 defect also involves the $E'3$ defect in $Ga_{1-x}Al_xAs$ (as suggested in Sec. V A) then, one must use $K=-\Delta+\delta_1$ since only the larger barrier, giving rise to the longest filling times, should be observed experimentally. In that case E_T, but not d_{FC}, is known and one must use d_{FC} as a fitting parameter. As shown in Fig. 15 a reasonable fit of the experimental data is obtained using $d_{FC}=160$ meV.

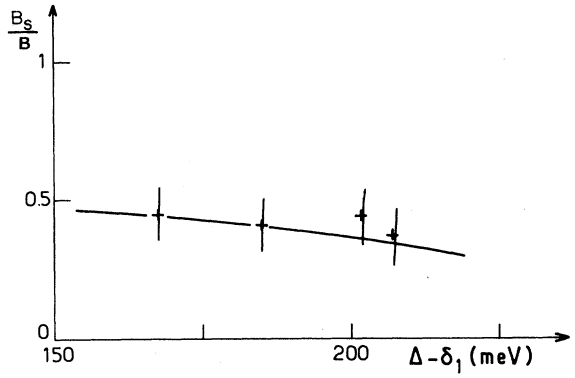

FIG. 15. Comparison between the expected variation (solid line) of the ratio B_S/B and the experimental data for the $SE4$ defect, assumed to correspond to the $E'3$ defect located in $Ga_{1-x}Al_xAs$ barriers.

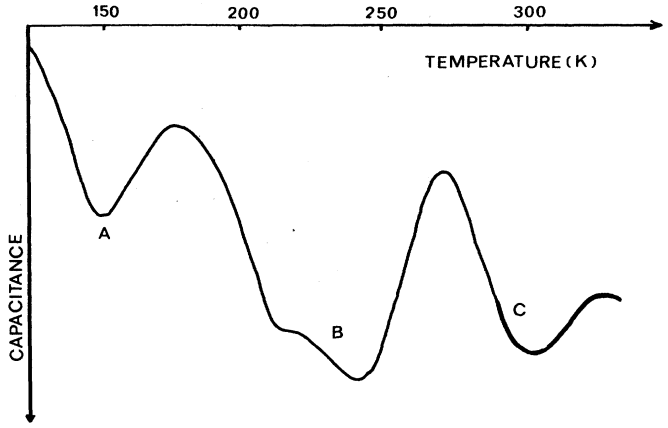

FIG. 16. High-temperature (100–350 K) DLTS spectrum in an unirradiated (5,5) structure (emission rate 106.5 s^{-1}).

In conclusion, the variation of the barrier height versus the superlattice band structure can be understood using the simple considerations developed above. However, owing to the low accuracy of the experimental data and the lack of determination of some of the parameters used, this picture cannot be verified quantitatively. For one defect ($SE4$) the expected variation of B_S versus band structure can be verified.

VI. NATIVE DEFECTS

Native defects have been looked for in unirradiated structures using DLTS in the range 4–300 K. This study has not been performed above room temperature because of the thermal stability of the contact. No defects have been detected in the (2,2), (3,3), and (4,4) structures for this temperature range. Thus, if the $EL2$ defect, a native defect in all GaAs materials, is present it cannot be detected. Indeed, its energy level being 0.75 eV below the conduction band in GaAs, giving rise to a DLTS peak around 400 K, its thermal emission in superlattices is expected to occur at a considerably larger temperature since its ionization energy will then be $0.75\ \text{eV}+\delta_1 \sim 0.85-0.9$ eV.

In the (5,5) structures DLTS detects, in addition to the series of peaks associated with emission of electron localized in the wells, three large peaks above 100 K, which we labeled A, B, and C (see Fig. 16). A similar structure is observed in the (4,2) structure but with a lower amplitude [for a comparison between the spectra obtained in the (5,5) and (4,2) structures see Fig. 17]. As discussed in Sec. III the minibands are destroyed by the electric field and thus these peaks should be related to localized levels situated in the wells or in the barriers which emit electrons in the corresponding conduction bands. The peak amplitudes in the (4,2) structure are smaller than in the (5,5) structure for two reasons: first, the width of the miniband being larger, the localization is weaker; second, the fraction of $Ga_{1-x}Al_xAs$ over GaAs layers is two times smaller. For instance, the B peak occurring around 220 K has a similar shape and the same signature (see Fig. 18), corresponding to an ionization energy of 465 meV, as the DX center in bulk $Ga_{1-x}Al_xAs$. It should therefore be ascribed to this defect and is consequently located in the $Ga_{1-x}Al_xAs$ barrier. We shall see elsewhere that this observation allows us to study the effect of the nature of the band structure on this defect. As we shall see below, peak C is associated with an ionization energy of ~ 0.80 eV and thus must be related to the presence of the $EL2$ defect in the wells. Finally, peak A exhibits an ionization energy of 290 meV. In principle, it is not possible to identify their nature as well as their location in wells or in barriers. However, since all the structures have been grown in an identical way, it is natural to think that the defects we observed in the (5,5) structure are also present in the (2,2), (3,3), and (4,4) structures. The fact that they are not observed when electrons are

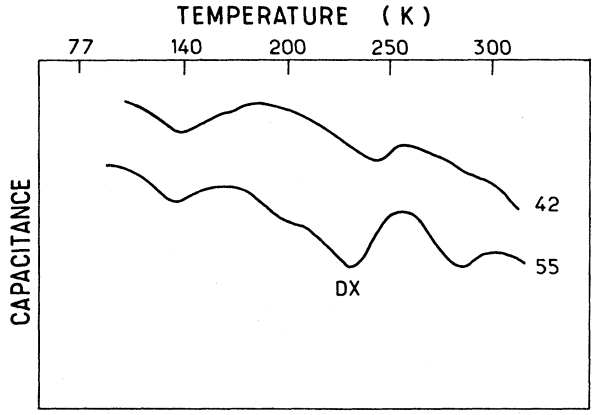

FIG. 17. Comparison between the high-temperature DLTS spectra in unirradiated (4,2) (emission rate 42.6 s^{-1}) and (5,5) (emission rate 21.3 s^{-1}) structures.

delocalized, i.e., when minibands exist, therefore implies that in this case the corresponding energy levels are deeper, i.e., that they lie in the GaAs wells. Indeed, the ionization energies are increased by δ_1 ($\sim$100 meV). As to the *DX* center, as we shall develop elsewhere, it is not detected in superlattices because its presence is directly linked to the *L* band and to the fact that this band contains four valleys, whose energy is shifted in the superlattice.[15]

These three peaks have already been observed: *A* at 0.28 (Ref. 16) or 0.35 eV (Ref. 17), *B* at 0.48 (Ref. 16) or 0.41 eV (Ref. 17), and *C* at 0.82 (Ref. 16) or 0.80 eV (Ref. 17) in the same type of superlattice (5,5) but with an alloy composition of 0.5 in the barriers. However, they have been interpreted assuming that there is no electric field induced localization.

As to the DLTS spectrum of the (4,2) structure it exhibits a structure similar to the (5,5) one but with a considerably lower amplitude presumably because the electric field induced localization is much weaker, the width of the first miniband being larger than in the (5,5) structure (see Table I).

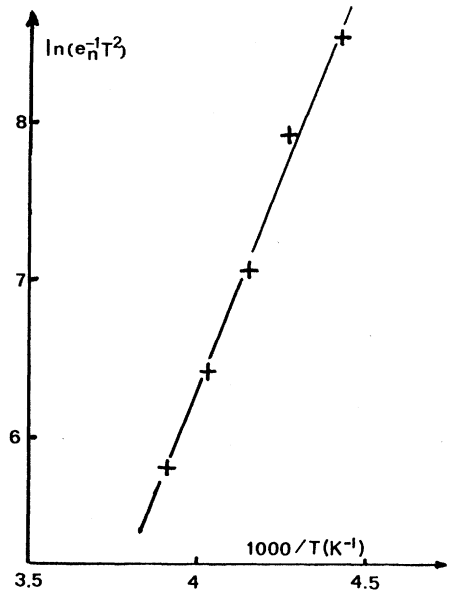

FIG. 18. Variation of the emission rate vs the inverse of the temperature for the *B* peak observed in a (5,5) structure.

VII. CONCLUSION

We have studied electron-induced defects in *n*-type-doped GaAs-$Ga_{1-x}Al_xAs$ superlattices. We have demonstrated that deep defects have energy levels and capture cross sections which can be deduced directly from the energy levels and capture cross sections the same defects have when they are in bulk GaAs and $Ga_{1-x}Al_xAs$, in agreement with simple theoretical considerations. This shows that the electrical characteristics of point defects in superlattices can be predicted once the characteristics of the defects in the bulk materials which compose the wells and the barriers are known thus providing the necessary understanding for the characterization of native defects. We have also briefly described the behavior of a superlattice in a variable electric field which gives a possible way to induce carrier emission from a defect into the superlattice miniband or into the original band minimum by varying the degree of localization of the carriers in the wells. This allows the study of possible band structure effects on deep levels.

ACKNOWLEDGMENTS

The authors are indebted to A. Regreny (CNET Lannion), who provided a few of the heterostructures used in the preliminary experiments. The Centre National de la Recherche Scientifique is "Associé à l'Université de Paris VII."

[1]J. C. Bourgoin, H. J. von Bardeleben, and D. Stiévenard, J. Appl. Phys. **64**, R65 (1988).

[2]D. V. Lang, in *Deep Centers in Semiconductors,* edited by S. T. Pantelides (Gordon & Breach, New York, 1986), Chap. 7.

[3]J. C. Bourgoin and M. Lannoo, in *Properties of Impurity States in Superlattice Semiconductors,* edited by C. Y. Fong, I. P. Batra, and S. Ciraci (Plenum, New York, 1988), p. 77.

[4]B. Deveaud, B. Lambert, B. Plot, A. Chomette, A. Regreny, J. C. Bourgoin, and D. Stiévenard, J. Appl. Phys. **62**, 3772 (1987).

[5]S. Y. Ren, J. D. Dow, and J. Shen, Phys. Rev. B **38**, 10677 (1988).

[6]D. Pons and J. C. Bourgoin, J. Phys. C **18**, 3839 (1985).

[7]D. V. Lang, R. A. Logan, and L. C. Kimerling, Phys. Rev. B **15**, 4874 (1977).

[8]J. C. Bourgoin, A. Mauger, D. Stiévenard, B. Deveaud, and A. Regreny, Solid State Commun. **62**, 757 (1987).

[9]S. L. Feng, J. C. Bourgoin, and G. G. Qin, Appl. Phys. Lett. **54**, 532 (1989).

[10]H. J. Huang, D. E. Ioannou, Z. Hatzopoulos, G. Kyriakidis, A. Christon, and N. A. Panpanicolaou, IOP Conf. Proc. Ser. No. **91** (IOP, Bristol, England, 1988), p. 541.

[11]D. J. As, P. W. Epperlein, and P. M. Mooney, IOP Conf. Proc. Ser. No. **91** (IOP, Bristol, England, 1988), p. 561.

[12]S. Loualiche, G. Guillot, A. Nouilhat, and J. C. Bourgoin, Phys. Rev. B **26**, 7090 (1982).

[13]D. Stiévenard, D. Vuillaume, J. C. Bourgoin, B. Deveaud, and A. Regreny, Europhys. Lett. **2**, 331 (1986).

[14]A. Chomette, B. Deveaud, M. Baudet, P. Auvray, and A. Regreny, J. Appl. Phys. **59**, 3835 (1986).

[15]J. C. Bourgoin, S. L. Feng, D. Stievenard, X. Letartre, E. Barbier, and J. P. Hirtz, Appl. Phys. Lett. **54**, 1115 (1989).

[16]P. A. Martin, K. Hess, M. Emanuel, and J. J. Coleman, J. Appl. Phys. **60**, 2882 (1986).

[17]S. Ababou, G. Brémond, P. Roura, L. Mayet, G. Guillot, and J. J. Coleman, in *Defects in Semiconductors,* Materials Science Forum, Vols. 38–41 (Trans Tech, Aedermannsdorf, Switzerland, 1989), p. 1397.